JOURNAL OF MAGNETIC RESONANCE **131,** 170–175 (1998)
ARTICLE NO. MN971275

The Effect of RF Power and Spinning Speed on MQMAS NMR

J-P. Amoureux,* M. Pruski,† D. P. Lang,† and C. Fernandez*

*Laboratoire de Dynamique et Structure des Matériaux Moléculaires, CNRS URA801, Université des Sciences et Technologies de Lille, F-59655 Villeneuve d'Ascq Cedex, France; and †Ames Laboratory, 230 Spedding Hall, Ames, Iowa 50011

Received June 13, 1997; revised January 13, 1998

It is known that the patterns of spinning sidebands observed in the multiple-quantum dimension of MQMAS spectra are often significantly wider than expected from the anisotropies of relevant interactions. It has been recently shown by others that these sidebands are generated due to the rotor-driven reorientations that the quadrupole tensors of the crystallites undergo during the evolution period between the multiple- and single-quantum conversion processes. We present an experimental and theoretical study of the effects of the spinning speed ν_R and RF field strength ν_{RF} on the development of these sideband patterns. The theoretical analysis relies upon numerical simulations and includes propagation of the density matrix during the entire MQMAS experiment. The possibility of additional rotational encoding during the RF pulses is discussed. Both the theoretical and experimental results show the benefits of using the highest available ν_R and ν_{RF}.

It has recently been demonstrated that a combination of two-dimensional multiple-quantum NMR with magic-angle spinning (MQMAS) can be used to remove the second-order quadrupolar broadening of the central transition of half-integer nuclear spins (*1*). The MQMAS method is now widely used to separate isotropic chemical shifts and second-order quadrupolar shifts. Several improvements to the original experiment have since been developed, aimed at increasing the efficiency of the multiple-quantum coherence excitation and at obtaining pure-phase 2D spectra (*2–7*). One of the approaches uses the $(0, \pm p, 0, -1)$ coherence transfer pathways, which are simultaneously selected by the appropriate phase cycling (*8*) of two strong RF pulses, followed by a selective ''softer'' 90° pulse: $H_1(\tau_1)_{\phi_1} - t_1 - H_2(\tau_2)_{\phi_2} - \tau - S(\tau_3)_{\phi_3} - t_2$, where H and S denote hard and soft pulses of duration τ_i and phase ϕ_i. The last part of this sequence $[-\tau - S(\tau_3)_{\phi_3}]$ makes up the so-called z filter, (*8, 9*) which removes the undesired transients from the observed signal and provides an easy and robust method for obtaining pure-phase spectra. The final selective 90° pulse allows the observation of the central-transition signal during t_2. Two-dimensional Fourier transformation with respect to t_1 and t_2 results in a spectrum from which the isotropic lineshape can be obtained by performing a shearing transformation or an appropriate skewed projection (*1, 2*).

Multiple spinning sidebands are frequently observed in the MQMAS spectra. Their number is usually much greater along the multiple-quantum (ν_1) than along the single-quantum (ν_2) dimension. More importantly, however, the overall width of the sideband pattern along ν_1 often exceeds the spectral range expected from direct rotational modulation of the interaction anisotropies during t_1, which is the ''classical'' origin of spinning sidebands in solid-state NMR. This phenomenon was recently reported and analyzed by Marinelli and Frydman (*10*), who concluded that it was due to rotor-driven reorientations that the quadrupole tensors of the crystallites undergo during the evolution period between the two H pulses. In their study, the MQMAS spectrum was calculated analytically from the powder-averaged evolution of the density matrix under the effect of the first-order quadrupolar Hamiltonian. The results of the numerical simulations and the sideband intensities measured for ^{23}Na ($S = \frac{3}{2}$) in polycrystalline sodium oxalate ($Na_2C_2O_4$) and sodium sulfate (Na_2SO_4) appeared in good agreement with the analytical predictions (*10*). This approach did not account for modulation of the quadrupole interaction during the strong RF pulses, however, because they last only a small fraction of the rotor period.

In this Communication we present an experimental and theoretical study of the sideband patterns in the MQMAS spectra as a function of the RF power level ν_{RF} and spinning speed ν_R used in the experiment. The theoretical analysis relies upon numerical simulations and includes propagation of the density matrix during the RF pulses. The benefits of using the highest available ν_R and ν_{RF} are discussed.

Figure 1 shows the isotropic projections of the 3QMAS spectra of $Na_2C_2O_4$ recorded for several values of ν_{RF} and ν_R. The experiments were performed at 9.4 T on a Chemagnetics Infinity spectrometer using a 3.2-mm Chemagnetics MAS probehead and the pulse scheme described above. The spectra, denoted 100/5, 100/10, . . . , 300/20, were acquired using three RF fields for the multiple-quantum conversions (ν_{RF} = 100, 200, and 300 kHz) and three rotation speeds (ν_R = 5, 10, and 20 kHz). The soft pulse was generated using $\nu_{RF} \cong 8.5$ kHz. To save experimental time, the t_1 evolution time was truncated at 1.3 ms, and only one phase

1090-7807/98 $25.00

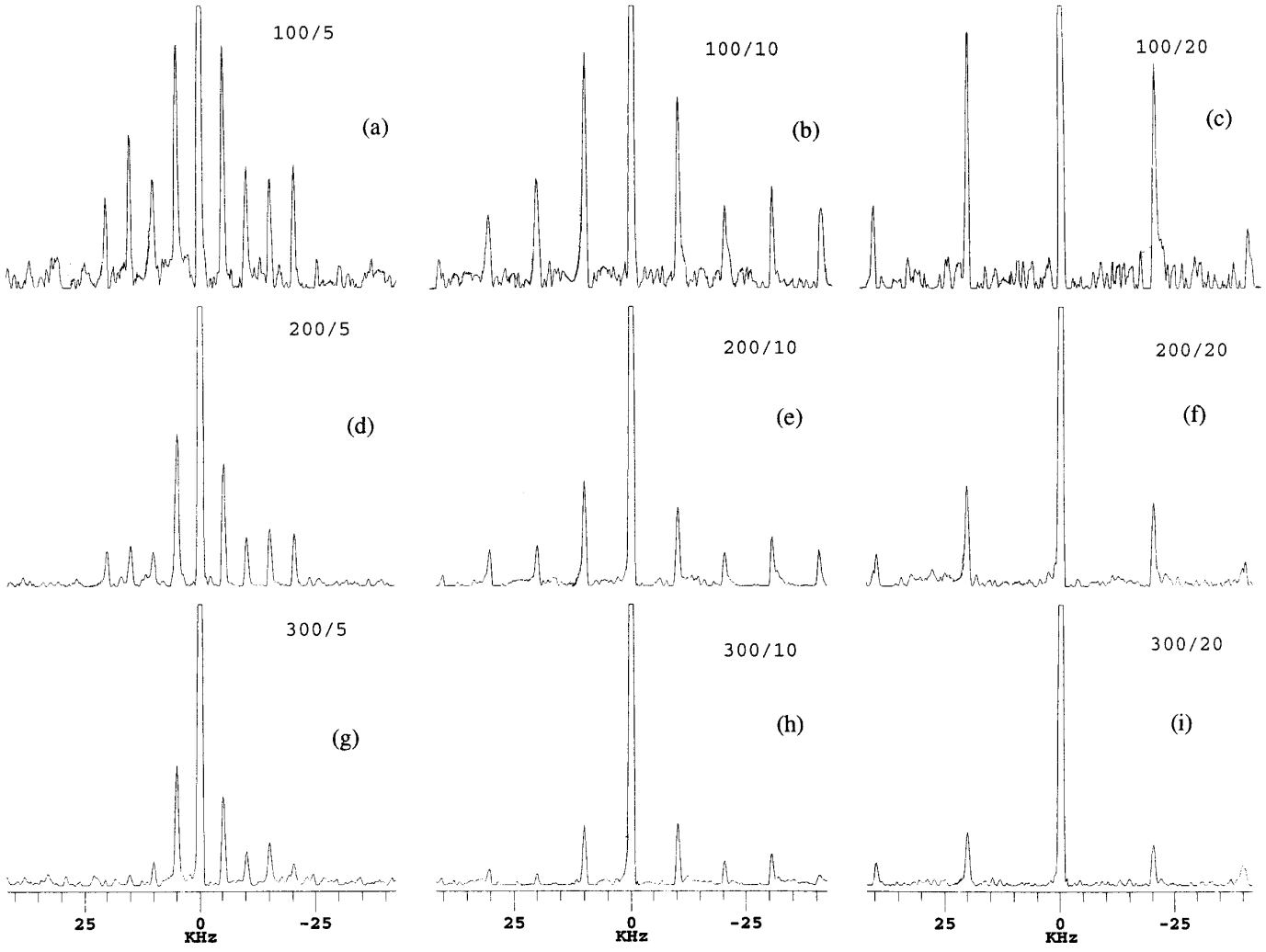

FIG. 1. Projections of sheared ^{23}Na 2D MQMAS spectra of $Na_2C_2O_4$ onto the isotropic axis. RF field ν_{RF} = 100 (a–c), 200 (d–f) and 300 (g–i) kHz; spinning speed ν_R = 5 (a, d, g), 10 (b, e, h), and 20 (c, f, i) kHz.

cycle was acquired for each t_1 increment. The height of each spectrum in Fig. 1 has been normalized to 25% of the maximum intensity of the centerband. Also shown, in Fig. 2, is the full 2D 3QMAS 100/5 spectrum of $Na_2C_2O_4$. As noted earlier (*10*), the number of sidebands along ν_1 is greater than along ν_2, despite the fact that at 9.4 T the second-order quadrupolar static linewidths in these two dimensions should be 10 and 12.4 kHz, respectively (*11*). The static NMR spectrum of the central transition of sodium in polycrystalline $Na_2C_2O_4$ is dominated by the quadrupole interaction with a coupling constant $C_Q = e^2qQ/h$ = 2.43 MHz and an asymmetry parameter η_Q = 0.77. This spectrum is only slightly broadened by the small shielding anisotropy and dipolar interactions (*12, 13*).

For a constant value of ν_{RF}, the spectra in Fig. 1 show a strong dependence on ν_R, which is in agreement with the previous work (*10*). More noticeable, however, are the changes in the sideband patterns obtained when ν_{RF} is varied and ν_R is kept constant. Comparison of spectra a, d, and g; b, e, and h; or c, f, and i indicates that (i) for a fixed spinning speed the number and relative intensity of the ν_1 sidebands decreases with increasing ν_{RF}, and (ii) the overall width of the sideband pattern increases at higher spinning speeds. Since our MQMAS experiments were independently optimized for each value of ν_{RF}, we must conclude that the observed changes originate from different evolution of the spin density matrix during the pulses. It is well known that the nutation behavior of quadrupolar spins depends on the RF power. Thus, even under optimized conditions, the 3Q coherences of ^{23}Na spins at $t = \tau_1$ strongly depend on ν_{RF}. This, in turn, must affect the sideband intensities, even if the only operable encoding process is due to the sample

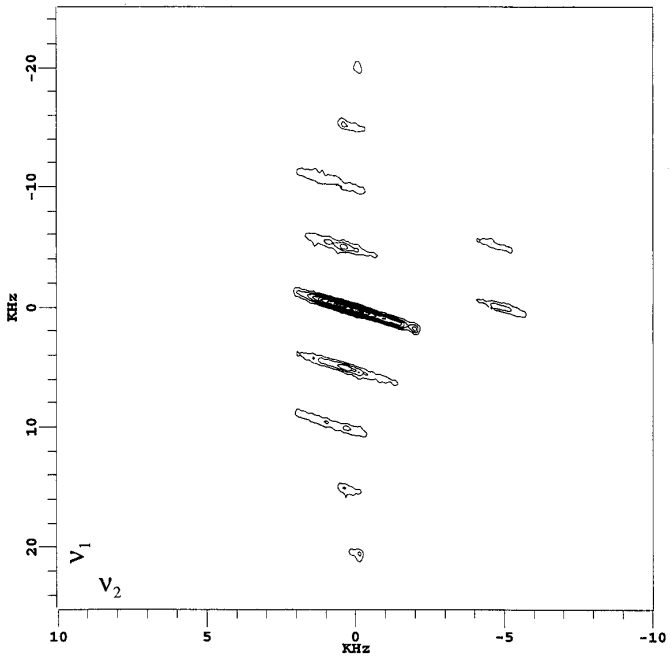

FIG. 2. Two-dimensional ^{23}Na unsheared 3QMAS spectrum of sodium oxalate acquired at 105.8 MHz, using $\nu_{RF} = 100$ kHz and $\nu_R = 5$ kHz.

reorientation during t_1, as described by Marinelli and Frydman (*10*). However, rotational modulation of the interactions responsible for the creation of the MQ coherences also occurs during the RF pulses. This indirect encoding process is considered below.

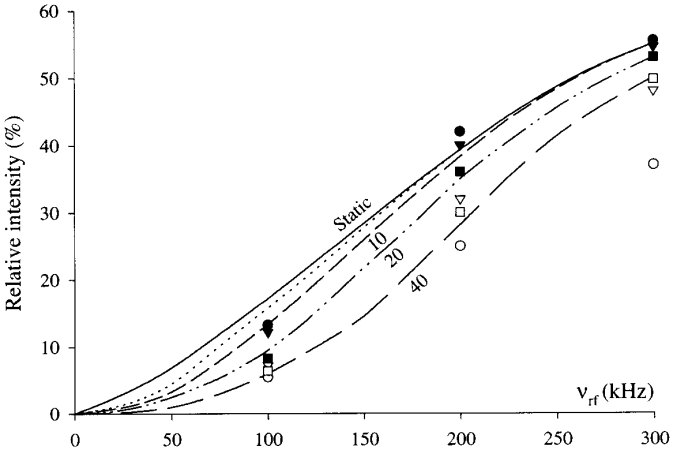

FIG. 3. Relative intensity in 3QMAS spectra of sodium oxalate ($\eta_Q = 0.77$, $C_Q = 2.43$ MHz) (*12, 13*) versus the RF field amplitude used for the first two pulses. Both H_{Q1} and H_{Q2} were included in the simulations. Curves have been computed assuming rectangular pulses with $\nu_0 = 105.8$ MHz, for static and rotating samples ($\nu_R = 5$, 10, 20, and 40 kHz). Experimental values are presented for the total (●, ▼, ■) and centerband (○, ▽, □) intensities with $\nu_R = 5$, 10, and 20 kHz, respectively. Small differences between numerical and experimental data are most likely due to pulse imperfections (phase glitches, RF field inhomogeneities, finite rise and fall times), and residual contributions from chemical shift anisotropy and dipolar effects.

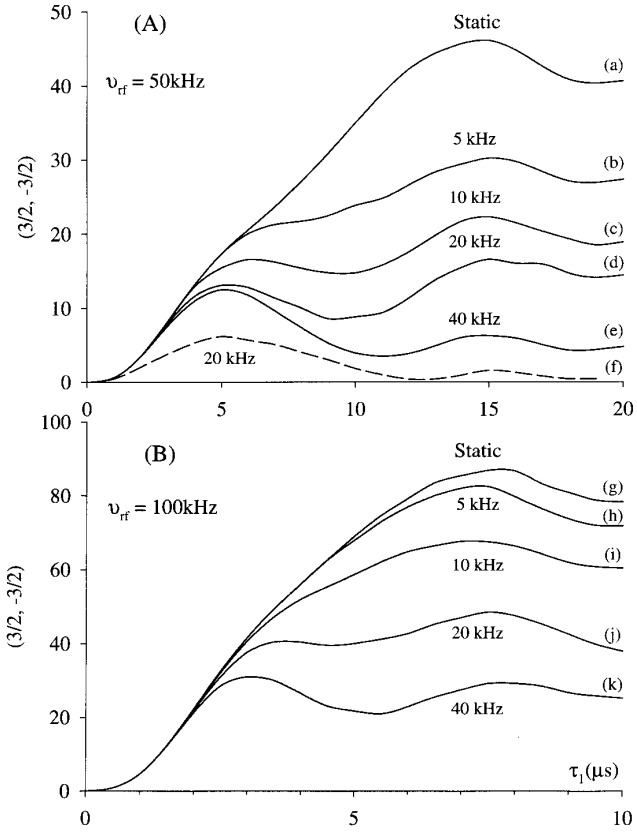

FIG. 4. Creation of 3Q coherences versus τ_1 and ν_R, for $S = \frac{3}{2}$ and $\nu_{RF} = 50$ (A) and 100 (B) kHz. Other parameters were the same as in Fig. 3, except curve f, for which $C_Q = 4.86$ MHz.

A PC-based program, PULSAR (*14*), was used to analyze the evolution of the spin density matrix in a rotating sample during the entire MQMAS experiment. The propagating of the density matrix results from the first (H_{Q1})- and second (H_{Q2})-order quadrupole interactions, as well as the RF Hamiltonians during the pulses. As a result of sample spinning, all these interactions are rendered time-dependent. Since the shielding and dipolar interactions are negligible in $Na_2C_2O_4$ (*12, 13*), they were excluded from the simulations. In the rotating frame, H_{Q1} is given by

$$H_{Q1}(t) = \bar{\nu}_Q(\alpha(t), \beta(t), \eta_Q)[S_z^2 - S^2/3], \qquad [1]$$

where $\bar{\nu}_Q$ and η_Q represent the quadrupole interaction and the asymmetry parameter, respectively. The two polar angles α and β describe the static magnetic field in the principal axis system of the electric-field tensor. Due to sample rotation, α and β are rendered time dependent. Similarly, H_{Q2} can be expressed in a general form

$$H_{Q2}(t) = A(\alpha(t), \beta(t), \eta_Q)S_Z + B(\alpha(t), \beta(t), \eta_Q)S_Z^3, \quad [2]$$

where $A(\alpha, \beta, \eta_Q)$ and $B(\alpha, \beta, \eta_Q)$ can be expressed in terms of the Wigner matrices (*14*).

The elements (m, m') of the density matrix of a quadrupolar spin system describe statistical coherences between Zeeman states $|m\rangle$ and $|m'\rangle$. The presence of a nonvanishing (m, m') element in the density matrix shows that there exists a coherent superposition of the quantum states $|m\rangle$ and $|m'\rangle$, with multiplicity defined by $m - m'$. Thus, the diagonal (D) elements of the density matrix (m, m), which represent the populations of the Zeeman levels, correspond to zero-quantum coherences. Let us denote the anti-diagonal elements $(m' = -m)$ by (AD) and the nondiagonal elements $(m' \neq \pm m)$ by (ND), respectively.

In the absence of relaxation processes and an RF field, the effects of first- and second-order quadrupolar interactions on the phase $\psi_{mm'}$ of an (m, m') coherence during time interval dt can be described as

$$\begin{aligned} d\psi_{mm'}(t) &= d\psi_1(t) + d\psi_2(t) \\ &= \bar{\nu}_Q(t)(m^2 - m'^2)dt + [A(\alpha, \beta, \eta_Q) \\ &\quad + B(\alpha, \beta, \eta_Q)(m^2 + mm' + m'^2)] \\ &\quad \times (m - m')dt. \end{aligned} \quad [3]$$

Clearly, the quadrupolar interaction has no effect on the zero-quantum coherences (i.e., D elements), whereas the AD and ND elements are dephased by second $(d\psi_2)$-order and first- and second-order $(d\psi_1$ and $d\psi_2)$ effects, respectively. Strong RF fields will, however, affect both the amplitude and the phase of all elements in the density matrix.

At equilibrium, the only nonzero elements of the density matrix are located along the diagonal. The 0Q → 3Q coherence transfers produced by the first-pulse can be approximately classified into two types of pathways. The primary contribution originates from the $|\pm\frac{1}{2}\rangle$ populations which quickly ''flow'' along or around the AD pathway, e.g., $(\frac{1}{2}, \frac{1}{2}) \rightarrow (\frac{1}{2}, -\frac{1}{2}) \rightarrow (\frac{3}{2}, -\frac{1}{2}) \rightarrow (\frac{3}{2}, -\frac{3}{2})$. Since H_{Q1} does not operate along most of this pathway, no substantial dephasing can occur during this pulse (τ_1 is typically on the order of a few microseconds) (*15*). In addition, a slower transfer occurs via alternative pathways involving several ND coherences, e.g., $(\pm\frac{3}{2}, \pm\frac{3}{2}) \rightarrow (\pm\frac{3}{2}, \pm\frac{1}{2}) \rightarrow (\pm\frac{3}{2}, \mp\frac{1}{2}) \rightarrow (\pm\frac{3}{2}, \mp\frac{3}{2})$. Considerable dephasing will occur in this case, since H_{Q1} can vary between zero and several megahertz, depending on the instantaneous orientation of the crystallite under consideration. As a result, for most crystallites the contributions of this pathway to the overall 3Q intensity is not very important. Even in the crystallites where H_{Q1} is sufficiently small at the beginning of the pulse to cause negligible dephasing in the static sample, this dephasing may increase strongly during τ_1 due to the change in orientation under high-speed MAS. Thus, important contributions via the ND pathways result only from those crystallites for which H_{Q1} remains small at all times during the first pulse.

It follows then, that for a given C_Q, a decrease in the MQMAS signal should be observed upon reducing the RF field (and, consequently, increasing τ_1) and/or increasing ν_R. The numerical calculations and experimental results of our work support this notion. For example, in Fig. 3 the relative intensity of the 3QMAS spectrum of ^{23}Na in sodium oxalate is shown as a function of ν_{RF} for various spinning speeds. In this figure, as well as in Figs. 4 and 6 discussed below, the numerical results are percentages of the intensity that can be obtained in a conventional experiment using a selective 90° pulse ($\nu_{RF} \ll C_Q$). While raising the RF field from 100 to 300 kHz benefits the MQMAS experiment by causing a four- to sevenfold rise in the total signal intensity, the effect of changing the spinning speed is somewhat ambiguous. Indeed, although both the numerical calculations and the experimental results show a notable decrease in total signal intensity with increasing ν_R, especially for lower values of ν_{RF}, the development of spinning sidebands depletes the integrated intensity of the centerband at slow spinning speeds. For this reason, the use of high spinning speeds remains more advantageous.

Figure 4 shows the simulated development of 3Q coherences in $Na_2C_2O_4$ as a function of τ_1 for the ν_{RF} fields of 50 and 100 kHz and for MAS speeds of up to 40 kHz. Clearly, the optimum value of τ_1 not only depends on the RF field used but also is strongly affected by the MAS speed (compare curves b and e in Fig. 4A). The two maxima present in most curves of Fig. 4 correspond to the intensities ''arriving'' via the two different pathways: the more efficient pathway around the AD (first maximum) and the less efficient one through the ND (second maximum). Finally, we note that the efficiency of the ND pathways strongly depends on C_Q, especially when a small RF field is used (compare curves d and f in Fig. 4A).

Those crystallites which do contribute to the 3Q coherences via the ND pathways will have their quadrupolar frequency affected by the sample rotation, i.e., at the end of the first pulse, the 3Q coherences can be partly modulated with the frequency ν_R. This supposition is corroborated by the numerical results of Fig. 5, which shows the simulated effect of changing τ_1 from 7.5 to 2.5 μs. Other parameters used in this simulation correspond to the 100/5 spectrum shown in Fig. 1a. Although the processes of rotational encoding during τ_1 and t_1 are not separable in this calculation, Fig. 5 shows that the length of the first pulse has a marked effect on the observed sideband pattern.

The results obtained for $S = \frac{3}{2}$ can be extended to other spin numbers and multiquantum orders. It has been shown (*16*) that for a fixed RF field, optimal τ_1 values are approxi-

mately proportional to $(2S + 1)^{-1}$. Thus, the rotational effects induced during the first pulse are expected to be at a maximum for $S = \frac{3}{2}$ and very small for $S = \frac{9}{2}$ (compare Figs. 4A and 6).

The transfer of the 3Q coherences toward the $|\pm\frac{1}{2}\rangle$ Zeeman populations is brought about by the second pulse. This process occurs mainly along the AD under a propagator that is represented solely by H_{Q2}. Thus, the optimal pulse duration τ_2 is smaller than τ_1 (*15*), and the corresponding dephasing $d\psi_2$ should not be as strongly affected by sample rotation. This conclusion is supported both by the simulations and the experimental results. First, the numerical calculations show that the loss of signal due to sample rotation occurs only during the first pulse. Second, while a change of τ_1 from 7.5 to 2.5 μs resulted in a spectrum with a greatly diminished sideband pattern at ν_{RF} = 100 kHz (Fig. 5), a similar simulation performed for the second pulse did not show any noticeable change in the lineshape. Note that due to the limited ND transfer, the spectrum of Fig. 5b is very similar to that observed with ν_{RF} = 300 kHz, see Fig. 1g. Clearly, when the highest available RF fields are used (Figs. 1g–1i) and, consequently, the *H* pulses become very short, the above-mentioned encoding process during τ_1 and τ_2 becomes insignificant. This limit case corresponds to the mathematical descriptions of Marinelli and Frydman (*10*). Finally, the experimentally observed lineshape along ν_2 (not shown) is independent of ν_{RF} and is close to the one observed using standard MAS.

While it is not obvious if a sideband analysis in the ν_1 dimension could become a simple diagnostic tool for probing the local nuclear interactions, the results of this work do have important practical significance. Since the experimental *S*/*N* ratio is determined by the centerband intensity and not by the total intensity, our analysis augments previous arguments regarding the need for using a combination of high RF fields and high spinning speeds (*15, 16*). For example, by using ν_{RF} = 300 kHz and ν_R = 20 kHz rather than ν_{RF} = 100 kHz and ν_R = 5 kHz, the centerband intensity observed for sodium oxalate was increased by a factor of 9 and the overall efficiency increased by 50%. This corresponds to a gain of ~80 in experimental time and, in addition, the resulting spectrum exhibits fewer spinning sidebands. Further improvement in *S*/*N* can be obtained by eliminating the sidebands along ν_1 via rotor synchronization (*17*). However, this technique limits the spectral width along ν_1 and thus requires high spinning speeds (*10*). This, in turn, may have a notable effect on the overall MQMAS intensity, except when using high RF fields (Fig. 3). Finally, we have shown that the spinning speed used in an MQMAS experiment affects the length of RF pulses required to optimize the signal.

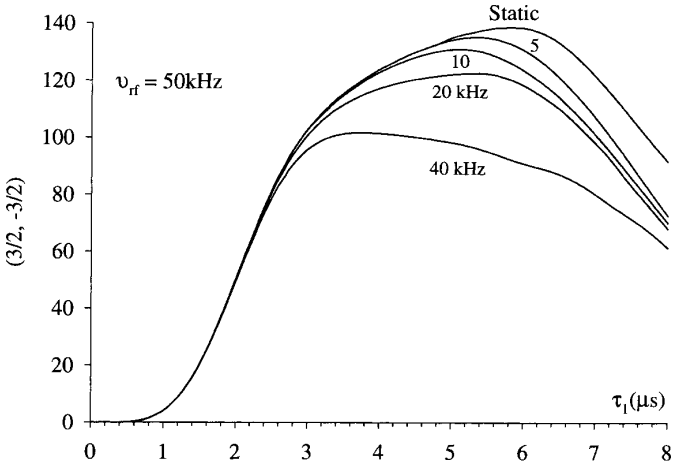

FIG. 6. Intensity of 3Q coherences versus τ_1 and υ_R, for $S = \frac{9}{2}$ and υ_{RF} = 50 kHz. Other parameters were the same as in Fig. 3, except that C_Q was set to 10 MHz in order to maintain the same spectral width along υ_2.

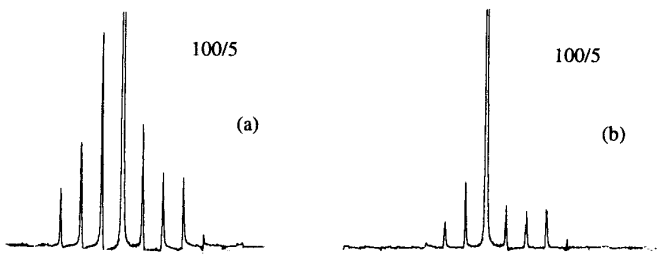

FIG. 5. Simulations of the isotropic 3QMAS spectra of $Na_2C_2O_4$ obtained for ν_{RF} = 100 kHz and ν_R = 5 kHz. Spectrum (a) τ_1 = 7.5 μs; spectrum (b) τ_1 = 2.5 μs. The height of these spectra has been normalized to 25% of the maximum intensity of the centerband.

ACKNOWLEDGMENTS

This research was supported at Ames Laboratory by the U.S. Department of Energy, Office of Basic Energy Sciences, Division of Chemical Sciences, under Contract W-7405-Eng-82, and at the University of Lille by the CNRS and the Region Nord-Pas de Calais.

REFERENCES

1. L. Frydman and J. S. Harwood, *J. Am. Chem. Soc.* **117,** 5367 (1995).
2. D. Massiot, B. Touzo, D. Trumeau, J. P. Coutures, J. Virlet, P. Florian, and P. J. Grandinetti, *Solid State NMR* **6,** 73 (1996).
3. G. Wu, D. Rovnyak, and R. G. Griffin, *J. Am. Chem. Soc.* **118,** 9326 (1996).
4. C. Fernandez and J. P. Amoureux, *Chem. Phys. Lett.* **242,** 449 (1995).
5. S. P. Brown, S. J. Heyes, and S. Wimperis, *J. Magn. Reson. A* **119,** 280 (1996).
6. S. P. Brown and S. Wimperis, *J. Magn. Reson.* **128,** 42 (1997).
7. M. Duer and C. Stourton, *J. Magn. Reson.* **124,** 189 (1997).

8. R. Ernst, G. Bodenhausen, and A. Wokaun, ''Principles of NMR in One and Two Dimensions,'' Oxford Univ. Press, New York (1987).

9. J. P. Amoureux, C. Fernandez, and S. Steuernagel, *J. Magn. Reson. A* **123,** 116 (1996).

10. L. Marinelli and L. Frydman, submitted.

11. J.-P. Amoureux, *Solid State NMR* **2,** 83 (1993).

12. K. T. Mueller, B. Q. Sun, G. C. Chingas, J. W. Zwanziger, T. Terao, and A. Pines, *J. Magn. Reson.* **86,** 470 (1990).

13. Y. Wu, B. Q. Sun, A. Pines, A. Samoson and E. Lippmaa, *J. Magn. Reson.* **89,** 297 (1990).

14. J.-P. Amoureux, C. Fernandez, and Y. Dumazy, *J. Chim. Phys.* **2,** 1939 (1995).

15. J.-P. Amoureux, C. Fernandez, and L. Frydman, *Chem. Phys. Lett.* **242,** 449 (1995).

16. J.-P. Amoureux and C. Fernandez, *Solid State NMR,* in press.

17. D. Massiot, *J. Magn. Reson. A* **122,** 240 (1996).